

High Resolution Vector Magnetograms With The Flare Genesis Vector Polarimeter

P. N. Bernasconi, D. M. Rust, H. A. C. Eaton

*JHU/Applied Physics Laboratory, 11100 Johns Hopkins Road, Laurel,
MD 20723-6099, USA*

Abstract. The Flare Genesis Experiment (FGE) uses an 80 cm balloon-borne solar telescope. By flying in the stratosphere, it is capable of acquiring high-resolution filtergrams and vector magnetograms of the solar photosphere and chromosphere, free of seeing induced aberrations. It carries an imaging vector polarimeter that uses a combination of two liquid crystal modulators and one linear polarizer and a lithium niobate Fabry-Perot etalon with 0.16 Å passband. The telescope successfully flew for 17 days in January 2000 over Antarctica, at an average altitude of 35 Km. Thousands of high spatial resolution, narrow-band images were recorded, and time series of H α filtergrams and photospheric vector magnetograms have been constructed. Of particular interest are the observations carried out on January 25 while the FGE was pointing at the newly formed active region NOAA 8844. We obtained a unique record of the magnetic field development related to new flux emergence. Several small flares were recorded during the development of the active region.

1. Introduction

The Flare Genesis Experiment (FGE) is a balloon-borne solar telescope designed to fly in the stratosphere over the Antarctic continent. It has an 80 cm primary mirror and theoretically is capable of 0.2 resolution. The goal of such an instrument is to acquire long time series high resolution vector magnetograms of solar active regions, unaffected by the seeing introduced by the Earth's atmospheric turbulence. The main focal plane instrument is an imaging vector polarimeter that records in sequence all components of the Stokes vector.

The principal objective of FGE is to advance our understanding of the origin of solar activity. Flares, coronal mass ejections, and coronal heating are caused by dissipation of energy associated with current-carrying magnetic flux ropes. The FGE concentrates on the study of the evolution of magnetic flux developments.

After the first flight in Antarctica on January 1996 (see Murphy et al. 1996) several modifications were introduced to improve the overall instrument performance (Bernasconi et al. 1999). In January 2000, the Flare Genesis Telescope flew above Antarctica for the second time. It was launched on January 10, 2000 from near McMurdo base and landed 17 days later on the Ross Ice Shelf about 340 km from McMurdo, after almost completing a full circle around the South

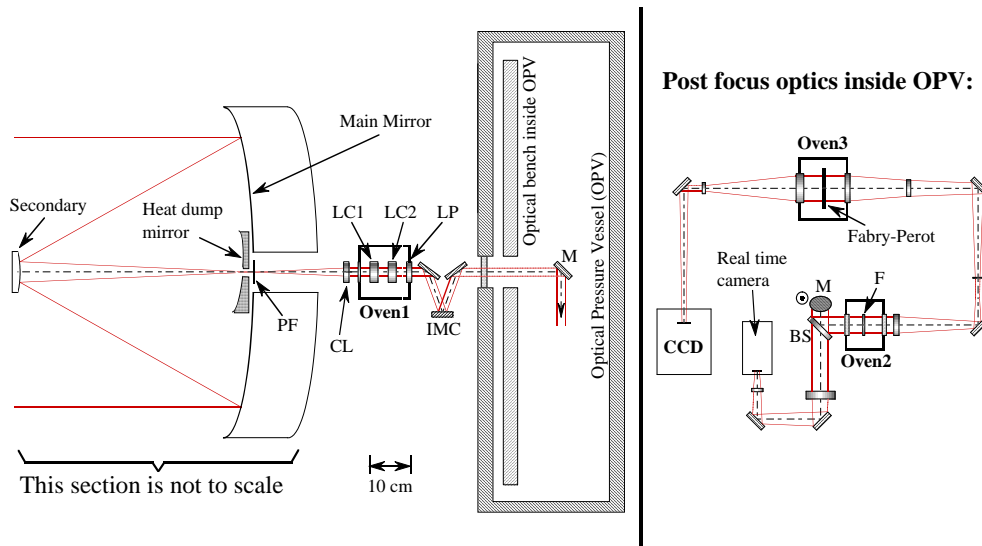


Figure 1. Schematic of the FGE optics: PF = primary focus; CL = collimating lens; LC1-2 = liquid crystal modulators; IMC = image motion compensator mirror; M = beam folding mirror inside OPV; BS = beam splitter; F = narrow band filter (1.6 Å bandpass).

Pole at an average altitude of 35 km. During the flight the instrument recorded about 50,000 images with a maximum resolution of $0''.5$.

In this article we will describe the FGE vector polarimeter and present some first results of the January 2000 flight. More details on the 1999/2000 Antarctic campaign can be found in the FGE web site (<http://sd-www.jhuapl.edu/FlareGenesis/>), while Bernasconi et al. (2000) gives a detailed description of the instrument behavior and performance during the flight. The main FGE characteristics and capabilities have also been presented by Rust et al. (1993, 1996), or on the web site above mentioned.

2. The FGE Imaging Vector Polarimeter

A schematic diagram of the FGE optics is shown in Fig. 1. The telescope is an 80 cm \varnothing F/1.5 Cassegrain with a diffraction limited resolution of $0''.2$ in the red. To compensate for the residual telescope pointing errors, typically in the order of $10''$ to $15''$ RMS, we designed an image motion compensation system (IMC) capable of stabilizing the image jitter at the CCD focus to about $0''.2$. The agile tip-tilt IMC mirror is located at an image of the entrance pupil and its actuators are steered according to the pointing error signals delivered by the pointing telescope sensor (a two axis lateral effect diode with an occulting disc covering 90% of the solar image on its center to increase its sensitivity). With the exception of the polarization analyzer and the IMC mirror the rest of the focal plane optics is located inside the optical pressure vessel (OPV), where a constant pressure of 1 atm was maintained throughout the flight. Ground-level

air pressure was required because we use high voltage to tune the passband of the Fabry-Perot filter (see below). It also allow the use of commercial grade electronics.

The polarization analyzer is located behind the collimating lens (CL), where the optics is still circularly symmetric, to minimize instrumental polarization. It is composed of two liquid crystal variable retarders (LC1 and LC2) followed by a linear polarizer (LP). The retardance can be tuned by varying the modulated voltage applied to the liquid crystal layers. Since the retardances of the liquid crystals also depend on their temperature, LC1 and LC2 are enclosed in an oven that controls and stabilizes their temperature to within 0.1° C. The fast axes of LC1 and LC2 are oriented parallel and at -45° , respectively, with respect to the linear polarization direction of LP, which was chosen to be set perpendicular to the positive Stokes Q direction. Six polarization measurements are required to record the full Stokes vector. Table 1 shows the retardance settings of the two liquid crystal retarders for the different polarization measurements.

Table 1. Retardances of the two liquid crystal retarders for the 6 Stokes measurements.

Measurement	$I + Q$	$I - Q$	$I + U$	$I - U$	$I + V$	$I - V$
Retardance LC1	0	0	$3/4\lambda$	$1/4\lambda$	0	$1/2\lambda$
Retardance LC2	$1/2\lambda$	0	$3/4\lambda$	$3/4\lambda$	$3/4\lambda$	$3/4\lambda$

The wavelength selection for the filtergrams is performed using the combination of a 1.5 \AA bandpass prefilter (F in Fig. 1) with a tunable lithium niobate Fabry-Perot etalon (Rust 1994) with 160 m\AA passband. Both filters are temperature controlled and stabilized. The prefilter has a fixed bandpass, so a series of different filters are mounted on a rotating wheel to allow observations at various wavelengths. The Fabry-Perot is tuned by applying a high voltage (max $\pm 3000 \text{ V}$) between its two face plates, and it can cover a wavelength range of about $\pm 1 \text{ \AA}$ from its neutral position. It is located at a secondary image of the entrance pupil to ensure a uniform spectral location of the passband across the entire focal plane field of view.

Finally, the detector at the focal plane is a 1024×1024 pixels 10 bits/pixel Kodak-Megaplex CCD camera with 20 MB/sec readout rate. The CCD field of view is about $100'' \times 100''$ with a pixel resolution of $0''.092$.

3. Data Acquisition and Reduction

The spectral line we selected to infer the vector magnetic fields is the CaI 6122 \AA line. This line is only moderately sensitive to Zeeman splitting ($g_{eff} = 1.75$), but relatively broad and better suited to the relatively broad passband of our Fabry-Perot etalon.

A full set of Stokes images is obtained by sequentially recording the six polarization states listed in Tab. 1 at the center of the blue and red wings of the CaI line. The integration time per frame is approximately 30 ms, and about

70 seconds are needed to acquire and store a full set of vector polarimetric measurements (12 images). The sequence is repeated every 3.5 minutes. Between each sequence three $H\alpha$ filtergrams are also recorded (at line core and at $\pm 0.8 \text{ \AA}$).

Every four hours the vector polarimetric observations are interrupted to perform a series of recalibration tasks, required by the periodic temperature change of the instrument due to the variation of the solar elevation during a 24 hour period. The telescope is refocused, and its heliographic coordinate system is recalibrated. The optimum integration times at the different wavelength are reestablished, and new dark current and flat field measurements are recorded. Finally, a series of measurements are performed by scanning with the Fabry-Perot across the CaI and $H\alpha$ lines. These scans are used in the post flight data reduction to calibrate the filtergrams wavelength.

The raw data are stored on-board into Exabyte tapes. A juke-box tape organizer holds 9 tapes for a total on-board storage capability of about 54,000 images.

The Stokes images Q/I , U/I , and V/I are calculated by applying to each image the standard dark current and flat field correction procedures, followed by the computation of the normalized difference between measurements of the opposite polarization states. E.g.: $Q/I = [(I+Q) - (I-Q)] / [(I+Q) + (I-Q)]$.

The magnetic field components longitudinal (B_{\parallel}) and transversal (B_{\perp}) to the line of sight (LOS) are then calculated following e.g. Ronan et al. (1987):

$$B_{\parallel} = L \times \frac{V}{T}, \quad B_{\perp} = T \times \sqrt[4]{\left(\frac{Q}{T}\right)^2 + \left(\frac{U}{T}\right)^2}, \quad (1)$$

where L and T are two constants that depend on the magnetic sensitivity of the spectral line used, on the exact location of the Fabry-Perot passband, and on the instrument polarimetric performance. We derive those constants by comparing the FGE B_{\parallel} and B_{\perp} values with the ones obtained by the Mees Imaging Vector Magnetograph (IVM) that during the flight was observing the same active regions as FGE. The IVM has a lower spatial resolution but it records full stokes profiles and the longitudinal and transversal field components are derived by means of an inversion code. The comparison shows that the best match between the FGE and IVM data are obtained with $L = 24000$ gauss and $T = 6000$ gauss.

The magnetic field inclination γ and azimuth χ are calculated as follows (see Ronan 1987):

$$\gamma = \arctan\left(\frac{B_{\perp}}{B_{\parallel}}\right), \quad \chi = \frac{1}{2} \arctan\left(-\frac{U/I}{Q/I}\right), \quad (2)$$

χ has another possible solution $\chi_1 = \chi + 180^\circ$, because of the 180° ambiguity introduced by the symmetry properties of the transverse Zeeman effect.

The next step is to transform the inclinations and azimuths into the local heliographic coordinate frame, where γ is the angle of the field with respect to the normal to the solar surface in the observed region, and χ is its azimuth relative to the local $E - W$ direction (positive is counterclockwise starting from W). To solve the 180° azimuth ambiguity we plan to use the ambiguity-free currents method developed for the HAO/NSO ASP vector magnetograms (see

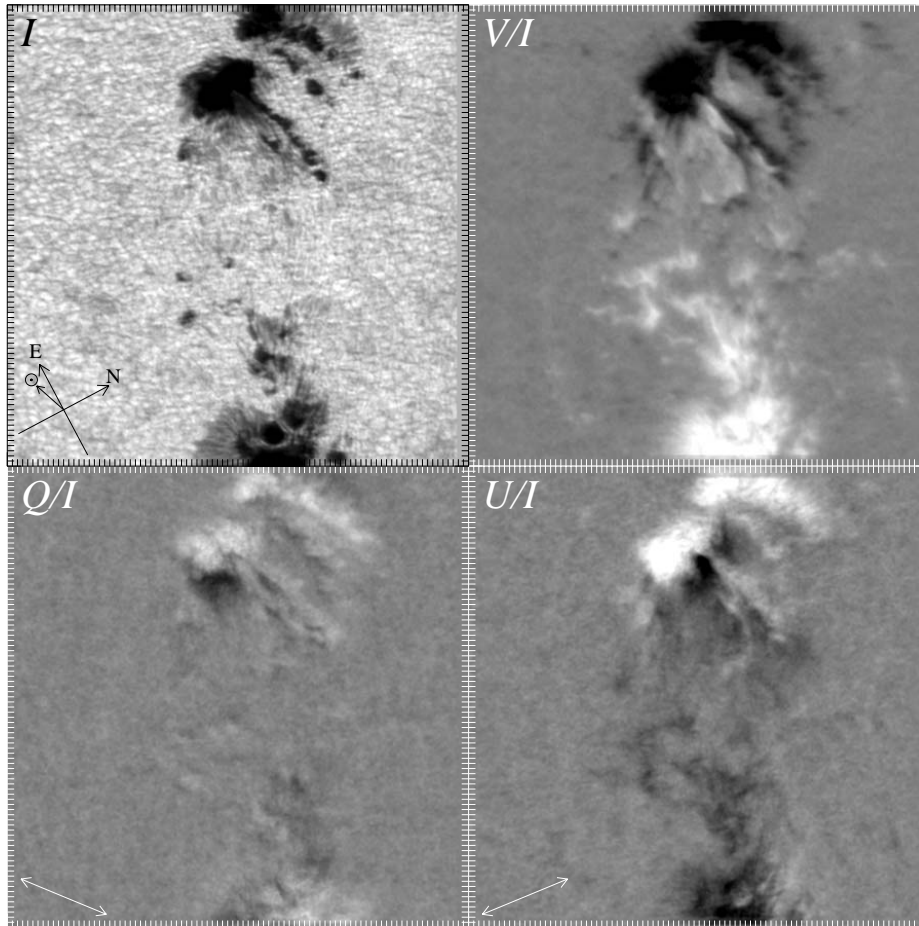


Figure 2. Example of Stokes filtergrams recorded by the FGE vector polarimeter. The Fabry-Perot filter was positioned at 6122.59 \AA in the red wing of the CaI 6122.5 \AA line. The field of view is $90'' \times 90''$ and the distance between tick marks is $1''$.

Skumanich and Semel 1996). This last step has not been implemented in our data reduction, yet. In the following we will only show the field orientation with respect to the LOS.

4. Flight Results

On January 25, 2000 (15 days into the second Antarctic flight) the entire instrument was working perfectly as it was targeting the young active region NOAA 8844. This region was a new flux emergence that appeared at the solar surface only two days earlier. On January 25 the active region was still very dynamic. The two opposite polarities were still moving apart from each other with relatively high speed, and new magnetic flux was constantly emerging from its center, approximately.

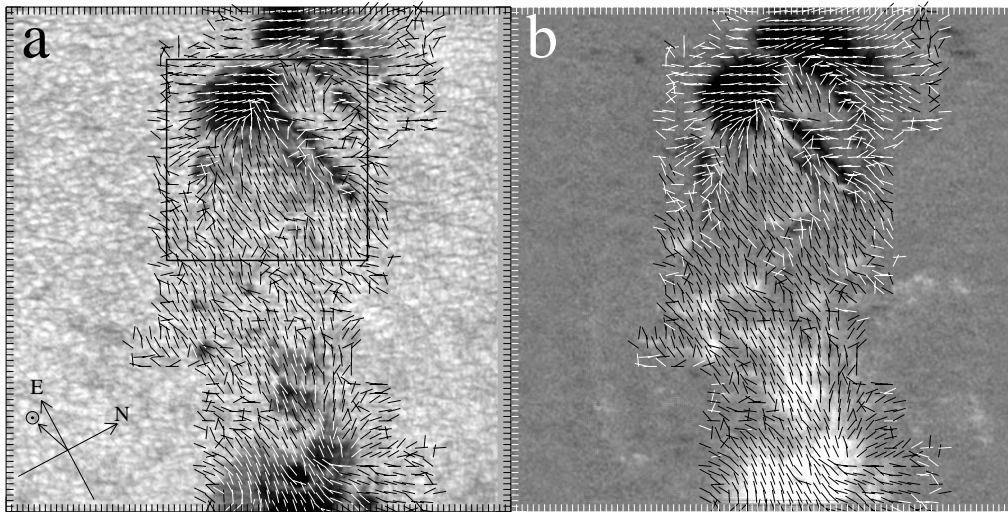


Figure 3. Example of LOS vector magnetogram derived from the FGE observations. (a) Orientation of the transversal field component plotted over the filtergram at 6122.5 Å. The black box indicates the area that is shown in detail in Fig. 4. (b) Transversal field orientation plotted over the LOS magnetogram. Pure white (black) corresponds to $+(-)$ 1400 Gauss. The tick mark separation is $1''$.

Figure 2 shows a typical set of vector polarimetric filtergrams of NOAA 8844 recorded by FGE. It is part of a 3.5 hour time series running from 15:49 UT to 19:20 UT. Stokes I and vector magnetogram movies as well as additional filtergrams and magnetic maps of the active region can be found in the FGE web site (<http://sd-www.jhuapl.edu/FlareGenesis>). On the lower left corner of the Stokes I filtergram are indicated the $N - S$ and $E - W$ direction as well as the Sun center direction \odot . On the Stokes Q and U filtergrams the orientation of the measured Q_+ and U_+ are shown. The observations in Fig. 2 were obtained at 17:32 UT, when the active region was located at approximately 7° N 27° W.

Following the reduction procedure described in Sec. 3 we obtained the LOS vector magnetogram shown in Fig. 3. The 6122 Å filtergram and magnetic movies show that the leading part of the active region (positive polarity; white in the magnetograms) was moving away from the center of the region faster than its trailing portion. The positive polarity flux nearby has a strong $E - W$ proper motion, plunging rapidly into the main leading spot. The field lines of the positive polarity are oriented nearly parallel to the horizontal motion of the magnetic patches (see Fig. 3b).

The most interesting and intriguing phenomena can be observed near the trailing sunspot. A detail of that region is shown in Figure 4. A supergranular cell, outlined with a dashed curve in Fig. 4a, is located right next to the spot. In the middle of the supergranule the emergence of mixed polarity magnetic flux can be observed. The small, freshly emerged, bipoles move rapidly, and without separating, towards the edges of the supergranule, where we observe a concentration of bipolar magnetic flux. The positive polarity sits on the inner edge of the

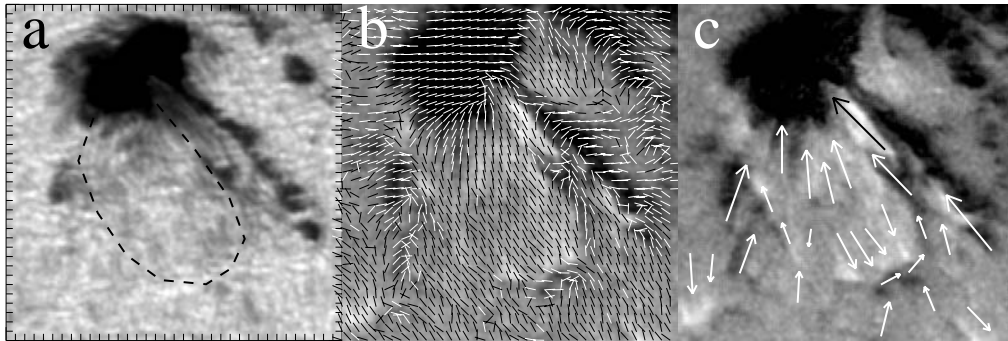


Figure 4. Detail of the LOS vector magnetogram shown in Fig. 3. (a) Filtergram at 6122.5 \AA . The dashed curve indicates the edge of a supergranular cell discussed in the text (tick mark separation: $1''$). (b) Vector magnetogram. (c) Longitudinal magnetogram with arrows indicating the horizontal magnetic flows.

supergranule, and the negative polarity on its outer edge. The magnetic patches then migrate “sideways” following the the edges of the supergranule and eventually get swallowed inside the negative polarity sunspot. The arrows in Fig. 4c show the observed flow of the magnetic flux (the length of the arrows is roughly proportional to the flow speed, which has not been quantitatively estimated, yet). A careful investigation of the transversal field direction (Fig. 4b) reveals that most of the field lines are oriented parallel to the motion of the magnetic features and also correspond with the direction of the dark filaments that can be seen in the photospheric filtergram (Fig. 4a) inside the supergranule. Furthermore, the observed motion of the magnetic features is also consistent with the photospheric gas flows observed in the 6122.5 \AA filtergrams.

Simultaneous filtergrams obtained by the FGE telescope at $H\alpha - 1 \text{ \AA}$ show the appearance of several brightenings of roughly $1''$ across. These brightenings are called in the literature Ellerman bombs (Ellerman 1917; Rust & Keil 1992) and mostly appear in young bipolar spot groups in the region between the two main magnetic concentrations of opposite polarity (like in the active region by us observed) or around large, mature sunspots. Most of the Ellerman bombs seen in our observations appear just ahead of the fast moving magnetic patches and move consistently together with them. We can also see a reoccurrence of “stationary” Ellerman bombs right at the edge of the supergranule cell, giving the impression of a pulsating chain of brightenings. Our observations are consistent with earlier studies of Ellerman bombs (Dara et al. 1997; Nindos & Zirin 1998) and confirm that they are intimately related with reconnection phenomena and fast motion of magnetic features.

Another interesting feature is a large, elongated magnetic patch of positive polarity that, at the beginning of the time sequence, was located west of the trailing sunspot (the white area underneath the black arrow in Fig. 4c). Its initial dimensions were roughly $8''4$ in length and $2''5$ at its maximum width. During the 3.5 hours movie it gets very rapidly swallowed into the spot and at the end of the sequence is almost completely disappeared. The nature of

this feature is still under investigation. It is possible that we witnessed the annihilation of a flux rope lying on its side, by the nearby young sunspot.

This is just a preliminary, phenomenological study of the evolution of the observed active region. We have started a careful analysis of the vector magnetogram and filtergram movies to understand the origin of the observed phenomena. We will also combine our data with joint observations by TRACE, SOHO, the Mees Observatory, and other observatories.

Acknowledgments. We are grateful to Kim Strohbehn, Bill Allmon, and Terry Harris for designing several key components of the FGE system. We thank Phil Wiborg for the development of the software for the autonomous observing program and for his support and advice. Brigitte Schmieder, Jeff Hickinbotham, and Nicholas Konidaris were part of the 1999/2000 Antarctic expedition. This work was supported by NSF under grant OPP-9615073 and by NASA grants NAG5-4955, NAG-5139, and NAG 8331. P. N. Bernasconi's work was partially supported by the JHU/APL Post-Doctoral Associates program.

References

- Murphy, G. A., Rust, D. M., Strohbehn, K., Eaton, H. A. C., Keil, S. L., & Keller, C. U., and Wiborg, P. 1996, *Proc. SPIE*, 2804, 141
- Bernasconi, P. N., Rust, D. M., Murphy, G. A., & Eaton, H. A. C. 1999, in *High Resolution Solar Physics: Theory, Observations, and Techniques*, T. Rimmele, K. S. Balasubramanian, and R. R. Radick (Eds.), *ASP Conference Series*, 183, 279
- Bernasconi, P. N., Rust, D. M., Eaton, H. A. C., & Murphy, G. A. 2000, in *Airborne Telescope Systems*, R. K. Melugin, H. P. Röser (Eds.), *Proc. SPIE*, 4014, 214
- Dara, H. C., Alissandrakis, C. E., Zachariadis, Th. G., & Georgakilas, A. A. 1997, *A&A*, 322, 653
- Ellerman, F. 1917, *ApJ*, 46, 298
- Nindos, A., & Zirin, H. 1998, *Sol. Phys.*, 182, 381
- Ronan, R. S., Mickey, D. L., & Orrall, F. Q. 1987, *Sol. Phys.*, 113, 353
- Rust, D. M. 1994, *Optical Eng.*, 33, 3342
- Rust, D. M., & Keil, S. L. 1992, *Sol. Phys.*, 140, 55
- Rust, D. M., Hayes, J. R., Lohr, D. A., Murphy, G. A., & Strohbehn, K. 1993, *Johns Hopkins APL Tech. Digest*, 14, 358
- Rust, D. M., Murphy, G. A., Strohbehn, K., & Keller, C. U. 1996, *Sol. Phys.*, 164, 403
- Skumanich, A., & Semel, M. 1996, *Sol. Phys.*, 164, 291